Headed Bar Connections between Precast Concrete Elements: Design Recommendations and Practical Applications

Jean Paul Vella[a], Robert L. Vollum[a], Raj Kotecha[b]

[a]Department of Civil and Environmental Engineering, Imperial College London, London, UK

[b]Laing O'Rourke, Dartford, UK

Abstract

The paper provides an overview of research into the design and behaviour of joints between precast concrete elements in which continuity of reinforcement is achieved through overlapping headed bars, allowing very short lap lengths. A series of tensile and flexural tests were carried out on joints with lapped headed bars of 25 mm diameter with 70 mm square heads and measured yield strength of 530 MPa. The tests studied the influence on joint behaviour of joint concrete strength, transverse reinforcement, geometry, and out-of-plane tolerances. Observations from tests and numerical analysis were used to develop design procedures for headed bar joints based on strut-and-tie modelling and the upper bound theorem of plasticity respectively. A recently completed project using headed bar joints demonstrates the benefits of using this system in precast concrete construction. The potential for further savings in costs and labour when adopting design recommendations stemming from this research is also discussed.

Keywords: Precast concrete, Headed reinforcement, Lap length, Strut-and-tie, Nonlinear finite element analysis.

1. Introduction

The paper presents design recommendations for narrow cast in-situ joints between precast concrete slabs in which continuity of reinforcement is achieved through overlapping headed bars, similar to those used by Laing O'Rourke (LOR) in their patented e6 floor system and shown in Figure 1. The use of headed bars allows very short lap lengths to be used in comparison with straight bar splices which facilitates highly efficient construction systems. The design recommendations are based on a research project carried out at Imperial College London [1] in which tests were made on tensile and flexural specimens having splices of 25 mm diameter headed bars with 70 x 70 x 16 mm friction welded heads. The net head bearing area was nine times the bar diameter which is sufficient to develop the full bar yield strength by bearing, without any contribution from bond along the bar [2, 3].

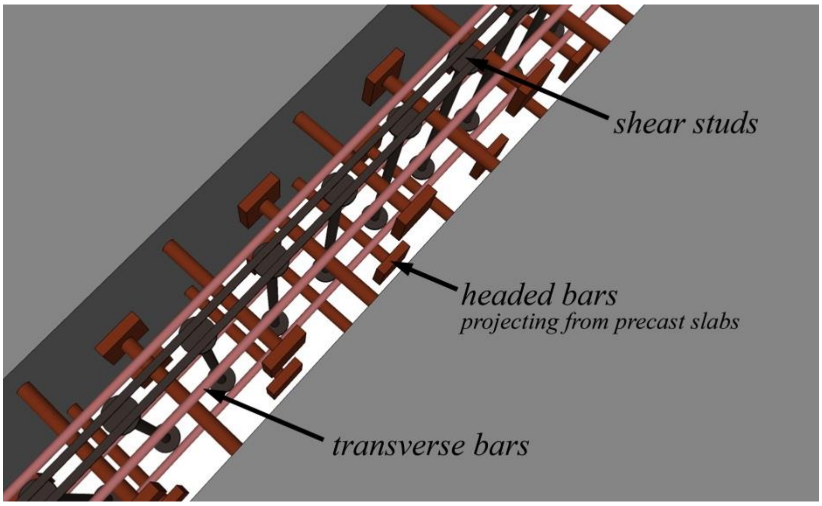

Figure 1: Typical headed bar joint

During construction of the e6 floor system, adjacent precast slabs can be temporarily supported off each other using easily handled steel brackets which eliminates the need for traditional propping with regular slab layouts. This allows follow-on trades to commence earlier, leading to significant savings in construction time. On-site labour is also significantly reduced, making construction sites safer whilst achieving a higher quality end product. The joint lies within the slab depth and therefore allows storey heights to be minimised in comparison with other common precast concrete construction systems.

Several studies have been made of short reinforcement splices using headed bars and overlapping U-bars of which the most pertinent are described below. Thompson et al. [4] performed flexural tests on lap splices using headed bars with small heads not capable of developing the full bar strength without contribution from bond. Their tests studied the influence on lap strength of variables including head size, lap length, bar spacing and confinement. Subsequently, Thompson et al. [5] proposed a design model for headed bar lap strength which combines models for head bearing capacity and bond. The model is applicable to anchorage lengths of at least six times the bar diameter which is greater than used in the e6 flooring system. Chun [6] tested beams with lapped large diameter headed bars and found lap strength to increase with concrete strength, lap length and provision of transverse reinforcement in the form of stirrups. In another study, Li et al. [7, 8] tested flexural specimens with lapped 16 mm diameter headed bars with 51 mm diameter heads capable of developing the full bar yield strength by bearing. For their tested detail, a lap of 152 mm developed the full bar strength with adequate ductility. Li and Jiang [9] developed a strut-and-tie model for determining the strength of headed bar splices, like those tested by Li et al. [7] , which gives reasonable predictions for their test specimens.

Short U-bar splices have been shown by several researchers [10-16] to be effective in tension. Ma et al. [13] tested 16 mm diameter U-bar splices in tension, with a minimum concrete cylinder strength of 48 MPa, and found lap strength to increase with concrete strength and lap length. They concluded that a lap length of 152 mm, with transverse bars inside the U-bars, is sufficient to develop adequate strength and ductility. He et al. [14] performed flexural tests on specimens with vertically oriented tight bend U-bars in the tensile zone and proposed a strut-and-tie model (STM) with which they determined the optimal spacing of U-bars to be twice the overlapping length. Joergensen and Hoang [15, 16] developed an upper bound plasticity model for U-bar splices which is also pertinent to headed bars.

2. Research programme

2.1. *Test specimen details*

A series of tensile and flexural specimens with overlapping headed bars were tested in the Structures Laboratory at Imperial College London to determine the effect on lap strength of variables including; concrete strength, transverse bar size and arrangement, confinement from shear studs, lap length and headed bar spacing. Main longitudinal lapped headed bars in all tested specimens were 25 mm in diameter with standard 70 x 70 x 16 mm square heads capable of developing the full bar yield strength by bearing at the head. Tensile test specimens were used to represent the flexural tensile zone in slabs since this facilitated construction, testing and numerical modelling allowing more variables to be investigated. The geometry of a typical tensile test specimen is shown in Figure 2 while Table 1 gives details of the 32 tested tensile specimens of which 27 have been reported previously [17]. The headed bars used in the tensile specimens were 400 mm in length, measured between the inside faces of the heads. The free ends of the headed bars were clamped to the test rig and load was applied at the end of the single headed bar as shown in Figure 2. Load was applied under displacement control at a rate of 0.2 mm per minute up to failure. More details can be found in references [1, 17]. The test IDs in Table 1 fully describe the specimen reinforcement arrangement and concrete strength. For example, G1-39-2H12:TT'-S-100-200:

" G1 " – Test group

" 39 " – Measured concrete cylinder strength at time of testing

" 2H12 " – Number and diameter of transverse bars

" TT' " – Position of transverse bars as indicated in Figure 2

" S " – Shear studs included

" 100 " – Lap length of headed bars

" 200 " – Spacing of headed bars

Table 2 gives the material properties of the reinforcement bars used in all tensile and flexural specimens. As shown in Table 1, the tensile specimens were divided into five groups. Specimens in groups 1 to 3 had the standard headed bar layout shown in Figure 2. With the exception of specimens in group 2, without shear studs, and specimen G1-39-2H25:TT'-10S-100-200, with 10 shear studs (see Figure 3), specimens had two transverse shear studs positioned as shown in Figure 2. Specimen G1-39-2H25:TT'-10S-100-200 was tested to determine if transverse bar anchorage was improved by providing shear studs along the anchorage, which was not the case. Groups 1 and 2 investigated the influence of concrete strength on lap strength for specimens with and without transverse shear studs while group 3 investigated the influence of transverse reinforcement area and arrangement. Headed bar spacing and lap length were varied in groups 4 and 5 respectively.

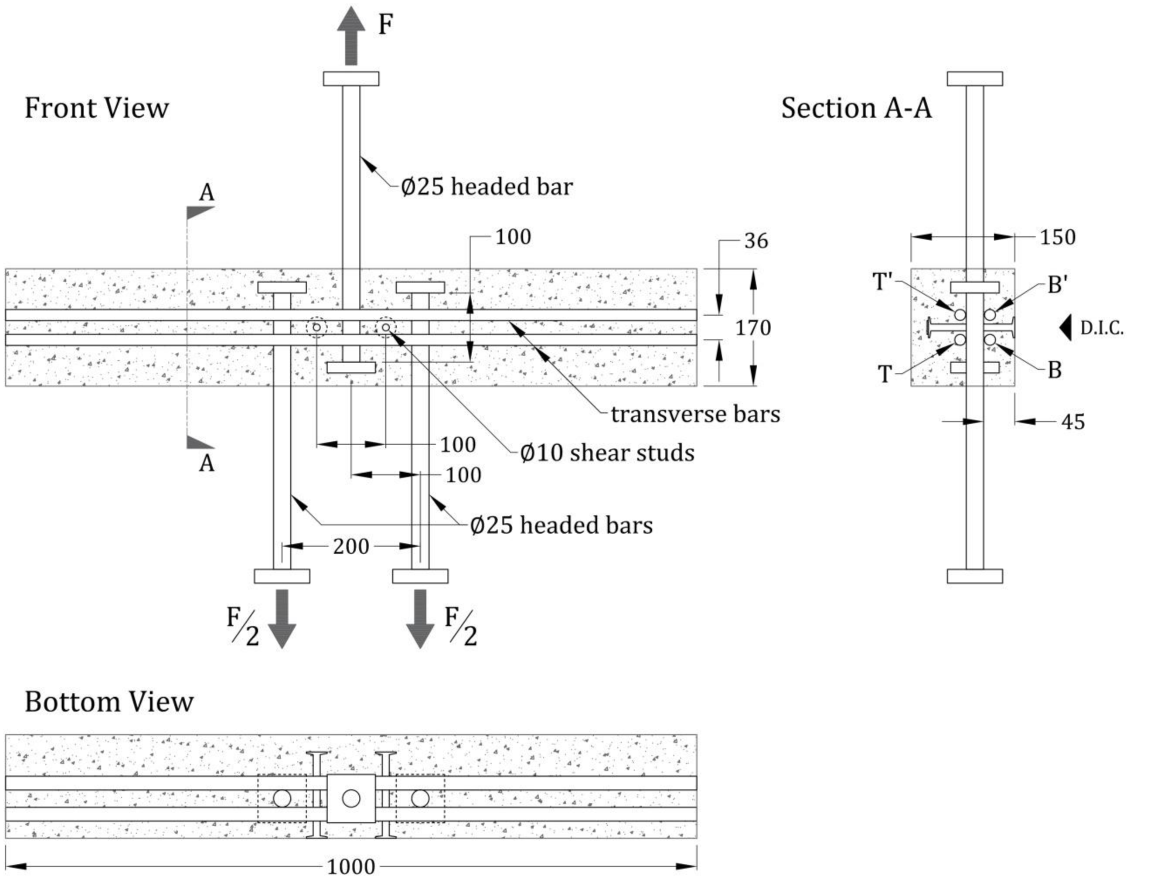

Figure 2: Typical tensile specimen geometry

Table 1: Tensile specimens measured and predicted mean strength

Test ID	P_{test} (kN) {failure mode}	P_{STM1} (kN) {failure mode}	P_{STM2} (kN) {failure mode}	P_{UB} (kN)	P_{NLFEA} (kN) {failure mode}	$\frac{P_{\text{test}}}{P_{\text{STM1}}}$	$\frac{P_{\text{test}}}{P_{\text{STM2}}}$	$\frac{P_{\text{test}}}{P_{\text{UB}}}$	$\frac{P_{\text{test}}}{P_{\text{NLFEA}}}$
G1-39-2H12:TT'-S-100-200	178 {J}	79 {T}	116 {T}	202	178 {J}	2.25	1.53	0.88	1.00
G1-26-2H16:TT'-S-100-200	149 {J}	137 {S}	142 {T}	133	174 {J}	1.09	1.05	1.12	0.86
G1-40-2H16:TT'-S-100-200	232 {J}	142 {T}	161 {S}	210	217 {J}	1.63	1.44	1.10	1.07
G1-54-2H16:TT'-S-100-200	259 {J}	142 {T}	209 {T}	283	247 {J}	1.82	1.24	0.92	1.05
G1-26-2H20:TT'-S-100-200	154 {J}	137 {S}	153 {S}	133	187 {J}	1.13	1.01	1.16	0.82
G1-40-2H20:TT'-S-100-200	242 {J}	188 {S}	223 {T}	210	232 {J}	1.29	1.08	1.15	1.04
G1-54-2H20:TT'-S-100-200	286 {Y}	223 {T}	223 {T}	283	263 {Y}	1.28	1.28	1.01	1.09
G1-48-2H25:TT'-S-100-200	260 {J}	214 {S}	286 {S}	250	265 {Y}	1.21	0.91	1.04	0.98
G1-39-2H25:TT'-S-100-200	274 {Y}	184 {S}	234 {S}	204	253 {J}	1.49	1.17	1.34	1.08
G1-39-2H25:TT'-10S-100-200	243 {J}	184 {S}	234 {S}	204	254 {J}	1.32	1.04	1.19	0.96
G2-39-2H12:TT'-100-200	159 {J}	79 {T}	116 {T}	174	164 {J}	2.01	1.37	0.92	0.97
G2-26-2H16:TT'-100-200	124 {J}	83 {S}	130 {S}	113	147 {J}	1.50	0.95	1.09	0.84
G2-40-2H16:TT'-100-200	181 {J}	131 {S}	142 {T}	179	196 {J}	1.38	1.27	1.01	0.92
G2-54-2H16:TT'-100-200	220 {J}	142 {T}	184 {S}	240	228 {J}	1.55	1.19	0.92	0.96
G2-26-2H20:TT'-100-200	133 {J}	83 {S}	130 {S}	113	159 {J}	1.61	1.02	1.17	0.84
G2-40-2H20:TT'-100-200	207 {J}	131 {S}	205 {S}	179	212 {J}	1.58	1.01	1.16	0.98
G2-54-2H20:TT'-100-200	257 {J}	176 {S}	223 {T}	240	254 {J}	1.46	1.15	1.07	1.01
G2-48-2H25:TT'-100-200	209 {J}	155 {S}	244 {S}	212	253 {J}	1.35	0.86	0.98	0.83
G3-28-2H20:TB'-S-100-200	236 {J}	144 {S}	165 {S}	144	218 {J}	1.64	1.43	1.64	1.08
G3-28-4H16:TT'BB'-S-100-200	264 {Y}	144 {S}	165 {S}	144	239 {J}	1.83	1.60	1.83	1.10
G3-28-4H20:TT'BB'-S-100-200	312 {Y}	144 {S}	165 {S}	144	274 {Y}	2.17	1.89	2.16	1.14
G3-46-2H20:TB'-S-100-200	316 {Y}	207 {S}	275 {Y}	240	288 {Y}	1.52	1.15	1.32	1.10
G3-46-4H16:TT'BB'-S-100-200	318 {Y}	207 {S}	275 {Y}	240	293 {Y}	1.53	1.16	1.32	1.09
G3-46-2H16:TB'-S-100-200	290 {Y}	207 {S}	275 {Y}	240	257 {J}	1.40	1.05	1.21	1.13
G3-48-1H25:T'-S-100-200	243 {J}	214 {S}	286 {Y}	250	243 {J}	1.14	0.85	0.97	1.00
G4-39-2H20:TT'-S-100-150	288 {Y}	254 {S}	302 {Y}	261	275 {Y}	1.13	0.96	1.10	1.05
G4-39-2H20:TT'-S-100-250	190 {J}	135 {S}	171 {S}	162	155 {J}	1.40	1.11	1.17	1.23
G4-39-2H20:TT'-S-100-300	130 {J}	99 {S}	139 {T}	132	111 {J}	1.32	0.93	0.99	1.17
G5-25-2H20:TT'-S-75-200	117 {J}	105 {S}	106 {S}	88	132 {J}	1.11	1.10	1.33	0.89
G5-25-2H20:TT'-S-150-200	213 {J}	196 {S}	257 {S}	213	209 {J}	1.09	0.83	1.00	1.02
G5-25-2H20:TT'-S-200-200	261 {J}	192 {S}	312 {Y}	299	213 {J}	1.36	0.84	0.87	1.23
G5-24-2H20:TT'-150-200	201 {J}	146 {S}	212 {S}	176	201 {J}	1.38	0.95	1.14	1.00
Mean						1.47	1.14	1.16	1.02
S.D.						0.293	0.239	0.270	0.108
C.o.V.						0.199	0.210	0.232	0.107

Note: J depicts joint failure, Y depicts headed bar yield, S depicts strut failure, T depicts tie failure.

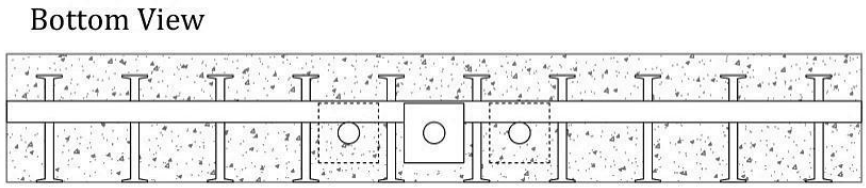

Figure 3: Specimen G1-39-2H25:TT'-10S-100-200 bottom view

Table 2: Reinforcement properties

Type	$\varnothing_b$ (mm)	Head size (mm)	f_y (MPa)	f_u (MPa)	E_s (GPa)
Headed bar	25	70 x 70 x 16	530	636	197
Headed bar	20	60 x 60 x 14	516	631	201
Headed bar	16	50 x 50 x 12	521	629	212
Straight bar	25	—	552	669	185
Straight bar	20	—	539	644	211
Straight bar	16	—	536	640	206
Straight bar	12	—	530	659	212
Straight bar	10	—	497	621	195
Shear stud	12	Ø36	564	656	223
Shear stud	10	Ø30	553	647	213

Four flexural specimens, (see Figure 4), were tested in four-point bending with the headed bar joint located in the tension zone of the constant moment region [18]. Load was applied via four independent hydraulic jacks, forming two line loads 600 mm apart, from the underside of the specimen fed by a single oil supply to maintain even pressure. This allowed digital image correlation to be used on the top tensile face of the specimen. Load was applied at a rate of approximately 10 kN/min. The specimens were supported with two fabricated steel beams anchored back into the laboratory strong floor to achieve a span of 2400 mm as shown in Figure 4. Further details are given in references [1, 18]. The slabs to either side of the joint were precast with the joint cast subsequently as an insitu stitch. The test results were compared with a control specimen with continuous bars through the joint. The flexural tests studied the influence on joint strength of concrete strength, shear studs and a 10 mm vertical out-of-plane offset of the precast planks. The specimens are described by their IDs as follows:

For example, B2-26-2H20-S-10:

“ B2 ” – Test group

“ 26 ” – Measured joint concrete cylinder strength at time of testing

" 2H20 " – Number and diameter of transverse bars

" S " – Shear studs included

" 10 " – Out-of-plane offset of precast planks

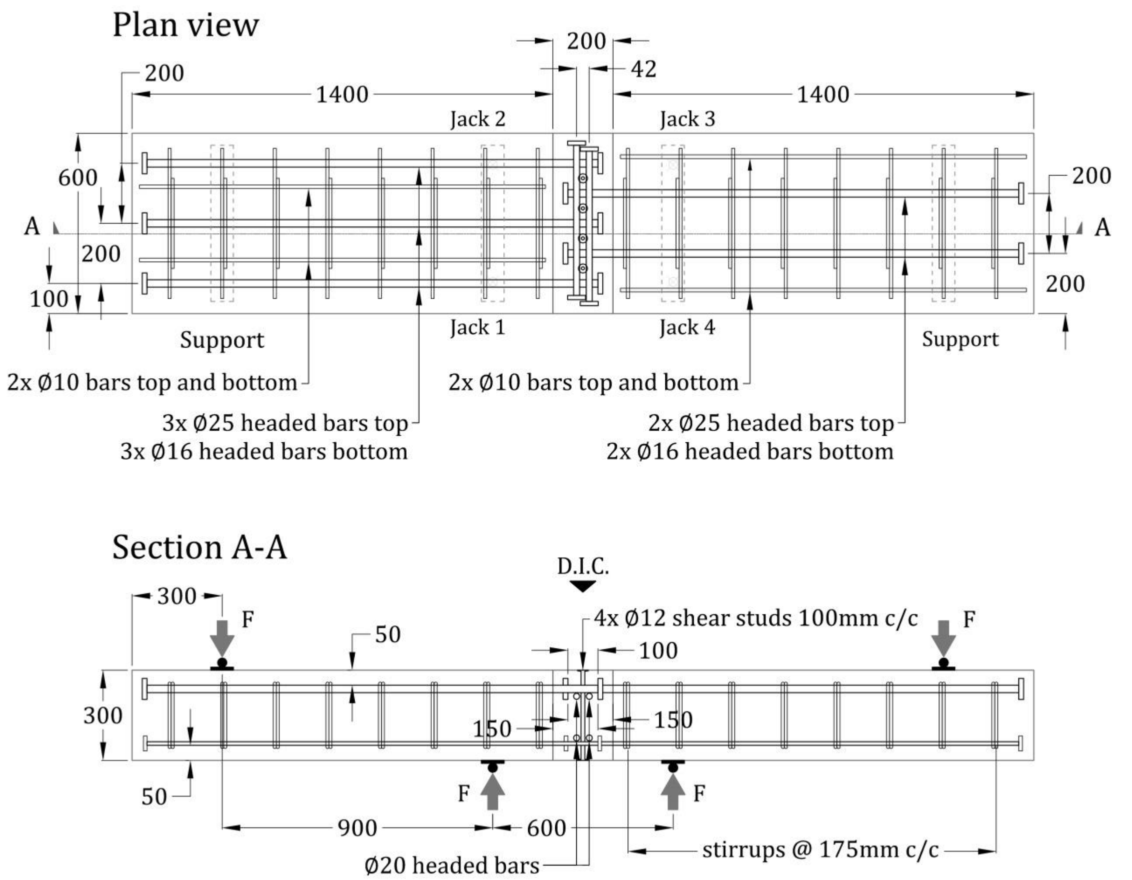

Figure 4: Typical flexural specimen geometry

Table 3: Flexural specimens measured and predicted mean strength

Test ID	M_{test} (kNm) {failure mode}	M_{STM1} (kNm)	M_{STM2} (kNm)	M_{UB} (kNm)	M_{NLFEA} (kNm)	$\frac{M_{\text{test}}}{M_{\text{STM1}}}$	$\frac{M_{\text{test}}}{M_{\text{STM2}}}$	$\frac{M_{\text{test}}}{M_{\text{UB}}}$	$\frac{M_{\text{test}}}{M_{\text{NLFEA}}}$
B1-39-/-/-/	160{Y}	N/A	N/A	N/A	N/A	N/A	N/A	N/A	N/A
B2-26-2H20-S-0	111{J}	82	82	66	95	1.35	1.35	1.68	1.17
B2-39-2H20-S-0	129{Y}	107	107	100	121	1.21	1.21	1.29	1.07
B2-24-2H20-/-0	84{J}	46	68	55	82	1.84	1.24	1.53	1.02
B2-26-2H20-S-10	99{J}	66	66	58	86	1.51	1.51	1.71	1.15
Mean						1.48	1.33	1.55	1.10
S.D.						0.235	0.119	0.166	0.059
C.o.V.						0.159	0.090	0.107	0.053

Note: M depicts failure moment at precast-to-joint interface, J depicts joint failure and Y depicts headed bar yield.

2.2. *Key observations and results from tests*

Tables 1 and 3 summarise the measured (test) and predicted joint strengths of the tension specimens (where P depicts failure load) and flexural specimens (where M depicts failure moment at the precast-to-joint interface) as well as associated failure modes. In tension test G3-28-4H16:TT'BB'-S-100-200, headed bar yield was achieved with a 100 mm lap using joint concrete with cylinder strength of 28 MPa, four 16 mm transverse bars and two 10 mm shear studs. Flexural yield was achieved in B2-39-2H20-S-0 with two top 20 mm transverse bars, 12 mm shear studs and joint concrete cylinder strength of 39 MPa. Crack widths in the flexural headed bar tests [18] were greatest at the precast-to-joint interface crossed by two headed bars, but still within the limit of 0.4 mm imposed by EC2 [19] at SLS for concrete inside buildings.

In tests where joint failure occurred prior to headed bar yield, joint strength of both tension and flexural specimens increased with concrete strength. However, flexural joint strengths were greater than estimated with section analysis from corresponding tension tests. Comparison of test results for similar specimens without and with shear studs shows that omission of shear studs resulted in reduced joint strength and ductility with the reduction proportionally greatest for flexure. The tension tests systematically investigated the effect of varying transverse bar diameter, number and arrangement. Joint strengths increased with transverse bar diameter up to, but not beyond, 20 mm with strengths in some cases reducing when the transverse bar diameter was increased from 20 mm to 25 mm. Providing transverse bars in the T' and B' positions (see Figure 2) in group 3 improved joint strength and ductility compared with comparable specimens in group 1 with transverse bars in the T and T' positions due to a change in failure mode. Ultimate failure of both tensile and flexural specimens with two transverse bars at the T and T' positions generally occurred by slippage of the central headed bar over the transverse bars with pullout of a partial concrete cone between the heads of the two supporting headed bars. Concrete pullout was more restrained in specimens with transverse bars above and below the headed bars, where the integrity of concrete within the lap zone was largely maintained at failure. Joint performance was further enhanced by increasing the number of transverse bars from two to four.

Reducing headed bar spacing and increasing lap length in tensile specimens (see groups 4 and 5) increased joint strength and ductility. A 10 mm out-of-plane offset within the joint of flexural specimen B2-26-2H20-S-10 did not significantly reduce joint strength compared to the companion specimen B2-26-2H20-S-0 with no offset.

Strain gauges were installed on some longitudinal headed bars, transverse bars and shear studs to determine axial and bending forces. Bending moments at the heads of lapped bars were found to be generally low and within 10% of the plastic moment capacity with the exception of flexural specimen B2-26-2H20-S-10 with 10 mm vertical offset where the bending moment reached 18% of the plastic capacity. In most cases, transverse bars did not yield. However, in both tensile and flexural tests, significant combined axial load and bending was measured in the transverse bars at the cross-over with the central longitudinal headed bar. Tensile stresses in shear studs at peak load were generally below 50% of yield. However, strains close to yield were recorded in the offset flexural specimen, indicating increased out-of-plane stresses within the joint. Further details can be found in references [17, 18].

3. Analytical models and nonlinear finite element analysis

3.1. Strut-and-tie model

LOR and Arup developed the STM shown in Figure 5 for three-bar tension tests which is depicted 'STM1'. Details of the model are given in references [1, 17]. This paper proposes an alternative STM denoted 'STM2' in which the calculation of diagonal strut strength is simplified.

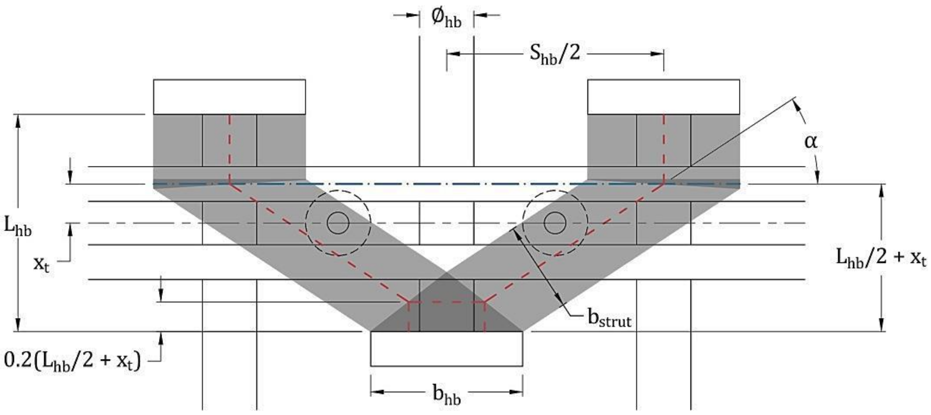

Figure 5: STM geometry

On plan STM2 has the same strut geometry as STM1. Struts are parallel sided and the central node height is assumed to be $0.4(L_{hb}/2 + x_t)$, where L_{hb} is the lap length between the insides of the heads, and x_t is the eccentricity of the transverse tie from the centreline of the joint (see Figure 5). For square heads and symmetrical joint geometry with no offsets in reinforcement positions, the strut width on plan perpendicular to its centreline is given by:

$$b_{\text{strut}} = 0.5 b_{\text{hb}} \sin\alpha + 0.4\left(\frac{L_{\text{hb}}}{2} + x_{\text{t}}\right)\cos\alpha \tag{1}$$

where b_{hb} is the width of the head and α is the angle between the diagonal strut and the transverse bar axis which is given by:

$$\tan\alpha = \frac{0.8(0.5L_{\text{hb}} + x_{\text{t}})}{0.5S_{\text{hb}} - 0.25b_{\text{hb}}} \tag{2}$$

where S_{hb} is the spacing of headed bars with same orientation.

The strut and tie forces N_{strut} and N_{tr}, respectively, are given by:

$$N_{\text{strut}} = {N_{\text{hb}}}/{2\sin\alpha} \tag{3}$$

and, $$N_{\text{tr}} = {N_{\text{hb}}}/{2\tan\alpha} \tag{4}$$

where N_{hb} is the force applied to the central headed bar.

In the absence of transverse shear studs, the strut depth in STM1 is taken as the head depth and the diagonal strut concrete strength as the concrete cylinder strength. In the presence of transverse shear studs, the depth and strength of the diagonal strut depends in a complex manner on the joint geometry and stud size [1, 17]. Test results show this approach to underestimate the unconfined diagonal strut strength while significantly overestimating the experimentally observed increase in strength due to shear studs [1, 17]. The strut strength in STM2 is calculated according to the provisions for partially loaded areas in ACI 318-14 [20] suggested by Tuchsherer et al. [21] for bearings not loaded over the full member width. Based on analysis of groups 1 and 2 with and without shear studs, a concrete strength efficiency factor of 0.85 is used for joints without shear studs, and 1.0 for joints with shear studs of at least 10 mm diameter and characteristic yield strength of 500 MPa. The resulting STM2 design strut capacity, C_{strut}, is calculated as:

$$C_{\text{strut}} = \begin{cases} f_{\text{ck}} A_1 \sqrt{A_2/A_1}/\gamma_{\text{c}} & \text{for joints with shear studs} \\ 0.85 f_{\text{ck}} A_1 \sqrt{A_2/A_1}/\gamma_{\text{c}} & \text{for joints without shear studs} \end{cases} \tag{5}$$

where $A_1 = h_{\text{strut}} b_{\text{strut}}$ and $A_2 = (h_{\text{strut}} + 2c_{\text{min}})(b_{\text{strut}} + 2c_{\text{min}}) \le 4A_1$. h_{strut} is the depth of the diagonal strut, which is equal to the head depth, b_{hb}, for aligned headed bars with square heads. c_{min} is the minimum cover available to the strut, f_{ck} is the characteristic compressive cylinder concrete strength, and

γ_c is the partial factor for concrete. The areas A_1 and A_2 are defined in Figure 6 for a headed bar splice with standard geometry.

Comparison of test results for B2-26-2H20-S-0 and B2-26-2H20-S-10 (see Table 3) shows that the strength of headed bar flexural splices is slightly reduced by vertical offsets arising from construction tolerances. The reduction in strength arises from the reduction in strut depth within the overlapping region of opposite heads (see Figure 7). STM1 accounts for the reduction in strut depth due to vertical offsets but also reduces the headed bar capacity to account for bending which is assumed to arise from eccentricity of loading [1]. The first two authors have previously shown [18] that headed bar bending did not significantly affect the strength of B2-26-2H20-S-10 with 10 mm out-of-plane offset. Consequently, the effect of vertical offsets is considered in STM2 through only the reduction in strut depth shown in Figure 7.

Only the T' and B' transverse bars in Figure 2 are considered to contribute to the transverse tie in STM1. In cases where transverse bar yield is calculated to be critical for the STM geometry shown in Figure 5, an alternative strut geometry can be checked in which all the transverse bars are assumed to be effective with bars positioned at their centroid as shown in Figure 8. In this case, for bars of equal diameter in both T (or B) and T' (or B') positions x_t is set to 0 mm (see Figure 5) in Equations (1) and (2). The resulting diagonal strut force may become critical due to the shallower strut angle. The design joint strength is considered to be the maximum of the values given by the STM geometries in Figures 6 and 8.

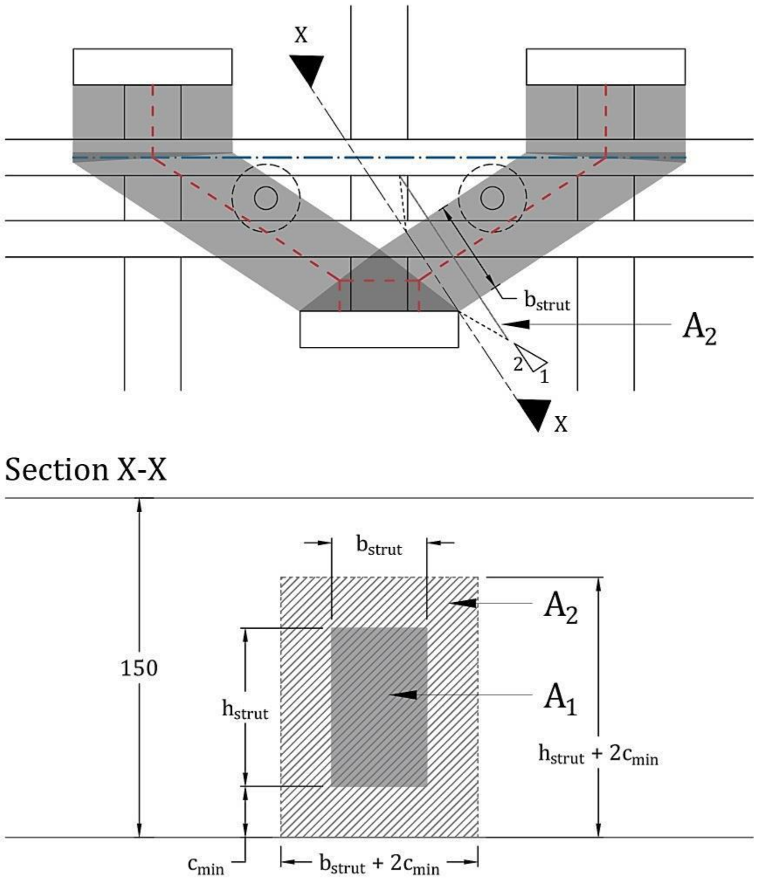

Figure 6: Definition of A_1 and A_2 in STM2

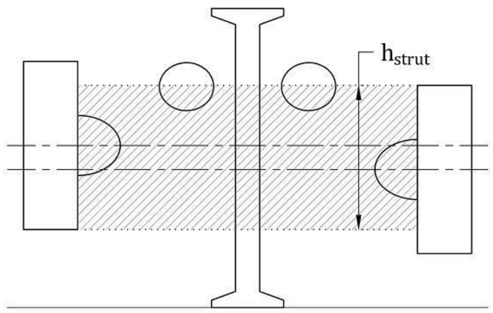

Figure 7: Section through diagonal concrete strut with headed bars offset out-of-plane

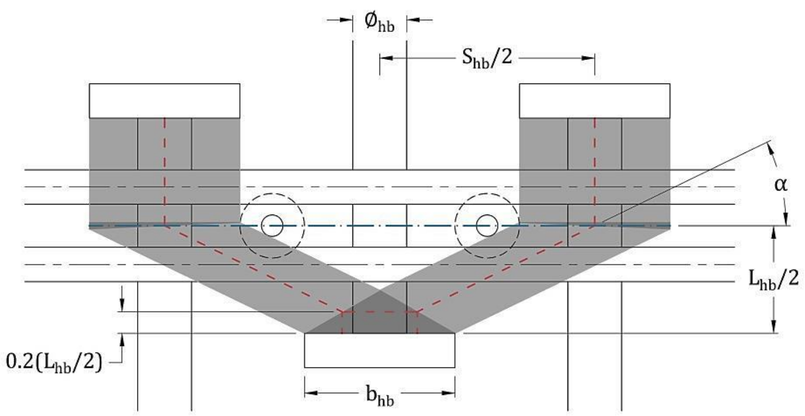

Figure 8: STM2 geometry with x_t = 0 mm

The transverse tie capacity, P_{tr}, is defined as:

$$P_{\mathrm{tr}} = n_{\mathrm{tr}}\, A_{\mathrm{tr}}\, f_{\mathrm{yk,tr}} / \gamma_{\mathrm{s}} \tag{6}$$

where n_{tr} is the number of bars contributing to the transverse tie which a maximum of 2 for the STM geometry of Figure 6 if transverse bars are in the T' and B' positions, or 4 for the geometry in Figure 8 which also includes the T and B bars. A_{tr} is the cross-sectional area of the transverse bars, $f_{\mathrm{yk,tr}}$ is the characteristic yield stress of the transverse bars, and γ_{s} is the partial factor for reinforcement.

The headed bar tensile capacity, P_{STM2}, is limited by the diagonal concrete strut, transverse bar, or headed bar strength (P_{hb}) as follows:

$$P_{\mathrm{STM2}} = \min \begin{cases} 2P_{\mathrm{strut}} \sin\alpha \\ 2P_{\mathrm{tr}} \tan\alpha \\ P_{\mathrm{hb}} \\ P_{sb} \end{cases} \tag{7}$$

where P_{sb} is the side blowout capacity calculated according to the fib recommendations [22].

As presented, both STM are applicable to laboratory controlled specimens, and allowance for specified tolerances would need to be accounted for in construction applications. Tables 1 and 3 give failure loads calculated for the tension (P) and flexural specimens (M) respectively using both STM with measured material properties and partial factors of 1.0. Table 1 shows that while less conservative than STM1, STM2 gives safe predictions of joint strength for all specimens in groups 1 to 3 except those with H25 transverse bars and concrete strength of 48 MPa. These tests are somewhat of an anomaly since increasing the transverse bar diameter from 20 mm to 25 mm resulted in lower joint strengths, contrary to the predictions of the STM. Additionally, the effect of transverse bar arrangement in group 3 specimens is not well captured by STM2, with calculated joint strengths only dependent on concrete strength. Changes in geometry in groups 4 and 5 also result in some overestimations of joint strength, especially for longer laps in group 5, possibly due to reduction of confinement provided by the shear studs in longer laps. Applying the 0.85 factor of Equation 5 for struts without shear studs to predictions for specimens G5-25-2H20:TT'-S-150-200 and G5-25-2H20:TT'-S-200-200, gives joint strengths of 218 kN and 273 kN respectively, which are very close to the measured strengths of 209 kN and 213 kN respectively. If the side blowout limit for headed anchorages of fib [22] is considered, the maximum joint strength of both specimens would be limited to 243 kN. The statistics at the bottom of Table 1 show that STM2 gives mean predictions closer to 1.0 than STM1 which is rather conservative. STM2 also gives reasonable predictions for the flexural specimens in Table 3 with very little scatter in results.

3.2. Upper bound plasticity model (UB)

An upper bound plasticity model based on that of Joergensen and Hoang for U-bar splices [15, 16] was considered as an alternative to the STM. The model, adapted to the headed bar geometry as shown in Figure 9, is described in references [1, 17], with the key equations reproduced below. Plane stress is considered with the limiting upper bound equation for joint strength, P_{UB}, being:

$$P_{\mathrm{UB}} = n_{\mathrm{L}} \nu f_{\mathrm{ck}} L_{\mathrm{hb}} b_{\mathrm{hb}} \left(\sqrt{r + \left(\frac{a}{L_{\mathrm{hb}}}\right)^2} - \frac{a}{L_{\mathrm{hb}}} \right) / \gamma_{\mathrm{c}} \quad (8)$$

where n_{L} is the number of headed bars at the least reinforced side of the joint, $a = S_{\mathrm{hb}}/2 - b_{\mathrm{hb}}$, and $r = 1$ for transverse reinforcement mechanical ratio $\Phi_T \geq 0.5\nu$. For lower values of Φ, r is given by:

$$r = 4\frac{\Phi_T}{\nu}\left(1 - \frac{\Phi_T}{\nu}\right) \quad (9)$$

$$\Phi_T = \frac{A_{\mathrm{s,tr}} f_{\mathrm{yk,tr}}}{L_{\mathrm{hb}} b_{\mathrm{hb}} f_{ck}} \quad (10)$$

As proposed for STM2, the concrete effectiveness factor, ν, is taken as 1.0 for joints with shear studs and 0.85 for joints without. Tables 1 and 3 show mean joint strength predictions calculated using the upper bound model (P_{UB} and M_{UB}) with measured material properties and partial factors equal to 1.0.

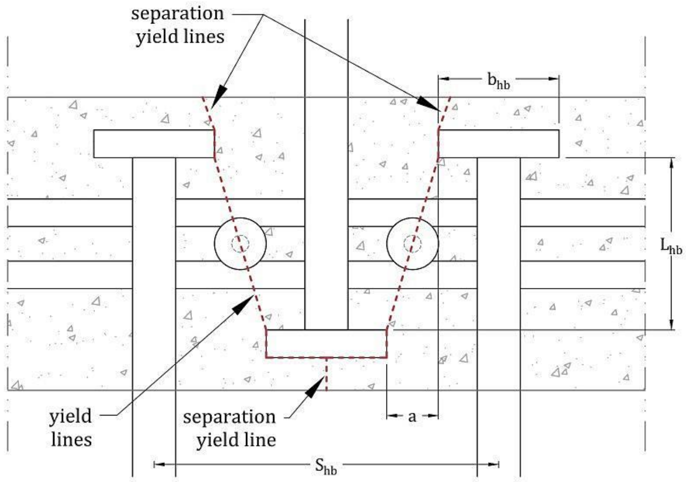

Figure 9: Upper bound model yield lines

Use of this upper bound model for specimens tested in this research results in $r = 1$ for all specimens, except G1-39-2H12:TT'-S-100-200, which makes strength predictions independent of the area and arrangement of the tested transverse bar arrangements. Generally, the joint capacity of specimens with high Φ_T ratio (e.g. group 3 tension specimens with 28 MPa concrete) is underestimated, while the capacity of joints with low Φ_T, i.e. with high concrete strength or small transverse bar area, is overestimated. As with STM2, the strength of specimen G5-25-2H20:TT'-S-200-200 with a 200 mm lap length is overestimated due to the high resistance provided by the long diagonal yield lines. However, the strength of this specimen is limited to 243 kN by side blowout according to the fib guidelines [22].

3.3. Nonlinear finite element analysis

Nonlinear finite element models (NLFEM) were developed for both the tensile and flexural joint specimens using the commercially available software ATENA-GiD [23] and calibrated against data from the tensile tests. Concrete was modelled with the "CC3DNonLinCementitious2" model available in ATENA which is a fracture-plastic model, combining constitutive models for tensile and compressive behaviour. Details are given in reference [24] and joint strength predictions from nonlinear finite element analysis (NLFEA) (P_{NLFEA} and M_{NLFEA}) using measured material strengths are given in Table 1 and 3 respectively. Overall, the NLFEA predictions closely follow the experimental results. Tensile joint strengths are generally overestimated for low strength joints, but marginally underestimated for joints with capacities close to the headed bar yield load, which are of most practical concern. Table 3 shows that good predictions were achieved for the tested flexural specimens, resulting in measured to predicted ratios greater than 1.0 in all cases.

4. Discussion and design recommendations

4.1. Joint design strength

In EC2 [19] design strengths are calculated in terms of characteristic material strengths using a partial safety factor format. According to EC0 [25], the 5% quantile of P_{test}/P_{calc} should be greater than 1.0 when evaluated with characteristic material strengths and partial factors equal to 1.0. The characteristic concrete compressive cylinder strength, f_{ck}, and the characteristic reinforcement tensile strength, f_{yk}, were calculated using Equations (11) and (12) respectively [3].

$$f_{\mathrm{ck}} = f_{\mathrm{cm}} - 8 \tag{11}$$

$$f_{\mathrm{yk}} = f_{\mathrm{ym}}/1.1 \tag{12}$$

where f_{cm} is the mean concrete compressive cylinder strength, and f_{ym} is the mean reinforcement tensile strength. Mean material strengths were considered equal to measured strengths. Tables 4 and 5 show the resulting characteristic joint strengths calculated for each analytical model ($P_{d,STM1}$, $P_{d,STM2}$ and $P_{d,UB}$) neglecting side blowout which was only critical for G5-25-2H20:TT'-S-200-200. Also included are characteristic strength predictions from NLFEA ($P_{d,NLFEA}$) obtained using the method of estimation of a coefficient of variation of resistance (ECOV) of fib Model Code 2010 (MC2010) [3]. When applying the ECOV method, concrete properties were generated within ATENA-GiD in terms of the characteristic concrete strength given by Equation (11).

Table 4 shows 5% quantiles of P_{test}/P_{calc} for each design method calculated assuming standard normal and log normal distributions of which log normal is most pertinent. The 5% log normal quantiles are all within an acceptable limit with values close to 1.0 as required by EC0 [25] and significantly greater than for the EC2 design method for punching shear [26]. Furthermore, comparison of characteristic joint strengths in Tables 4 and 5 suggests that laps were weaker in tension than flexural specimens in which the tested joint configuration is typically used. This is thought to be due to secondary bending induced by the three bar tension specimen arrangement. In light of this, and the ductile nature of headed bar lap failure, the characteristic strengths shown in Table 4 are considered acceptable for design.

Table 4: Tensile specimens predicted characteristic strength

Test ID	P_{test} (kN) {failure mode}	$P_{\text{k,STM1}}$ (kN) {failure mode}	$P_{\text{k,STM2}}$ (kN) {failure mode}	$P_{\text{k,UB}}$ (kN)	$P_{\text{k,FEA}}$ (kN)	$\frac{P_{\text{test}}}{P_{\text{k,STM1}}}$	$\frac{P_{\text{test}}}{P_{\text{k,STM2}}}$	$\frac{P_{\text{test}}}{P_{\text{k,UB}}}$	$\frac{P_{\text{test}}}{P_{\text{k,FEA}}}$
G1-39-2H12:TT'-S-100-200	178{J}	72{T}	106{T}	162	149	2.48	1.68	1.10	1.19
G1-26-2H16:TT'-S-100-200	149{J}	105{S}	105{S}	92	130	1.42	1.42	1.63	1.15
G1-40-2H16:TT'-S-100-200	232{J}	129{T}	129{T}	169	186	1.80	1.80	1.37	1.25
G1-54-2H16:TT'-S-100-200	259{J}	129{T}	185{S}	241	219	2.00	1.40	1.07	1.18
G1-26-2H20:TT'-S-100-200	154{J}	105{S}	105{S}	92	139	1.47	1.47	1.68	1.11
G1-40-2H20:TT'-S-100-200	242{J}	156{S}	193{S}	169	200	1.55	1.25	1.43	1.21
G1-54-2H20:TT'-S-100-200	286{Y}	203{T}	203{T}	241	240	1.41	1.41	1.19	1.19
G1-48-2H25:TT'-S-100-200	260{J}	182{S}	237{T}	208	237	1.43	1.10	1.25	1.10
G1-39-2H25:TT'-S-100-200	274{Y}	152{S}	186{S}	162	210	1.81	1.47	1.69	1.30
G1-39-2H25:TT'-10S-100-200	243{J}	152{S}	186{S}	162	214	1.60	1.30	1.50	1.14
G2-39-2H12:TT'-100-200	159{J}	72{T}	106{T}	138	132	2.21	1.50	1.15	1.20
G2-26-2H16:TT'-100-200	124{J}	57{S}	89{S}	78	105	2.18	1.39	1.59	1.18
G2-40-2H16:TT'-100-200	181{J}	105{S}	129{T}	143	154	1.73	1.40	1.26	1.18
G2-54-2H16:TT'-100-200	220{J}	129{T}	157{S}	205	191	1.70	1.40	1.07	1.15
G2-26-2H20:TT'-100-200	133{J}	57{S}	89{S}	78	114	2.34	1.49	1.71	1.17
G2-40-2H20:TT'-100-200	207{J}	105{S}	164{S}	143	170	1.97	1.26	1.44	1.22
G2-54-2H20:TT'-100-200	257{J}	150{S}	203{T}	205	212	1.72	1.27	1.25	1.21
G2-48-2H25:TT'-100-200	209{J}	129{S}	203{S}	177	200	1.62	1.03	1.18	1.05
G3-28-2H20:T'B'-S-100-200	236{J}	112{S}	118{S}	103	158	2.11	2.01	2.30	1.49
G3-28-4H16:TT'BB'-S-100-200	264{Y}	112{S}	118{S}	103	185	2.36	2.25	2.57	1.43
G3-28-4H20:TT'BB'-S-100-200	312{Y}	112{S}	118{S}	103	220	2.79	2.65	3.04	1.42
G3-46-2H20:T'B'-S-100-200	316{Y}	175{S}	227{S}	198	239	1.80	1.39	1.59	1.32
G3-46-4H16:TT'BB'-S-100-200	318{Y}	175{S}	227{S}	198	259	1.81	1.40	1.60	1.23
G3-46-2H16:T'B'-S-100-200	290{Y}	175{S}	227{S}	198	223	1.65	1.28	1.46	1.30
G3-48-1H25:T'-S-100-200	243{J}	182{S}	237{T}	208	190	1.34	1.03	1.17	1.28
G4-39-2H20:TT'-S-100-150	288{Y}	210{S}	237{T}	208	231	1.37	1.22	1.39	1.25

G4-39-2H20:TT-S-100-250	190{J}	112{S}	148{S}	129	138	1.70	1.29	1.47	1.38
G4-39-2H20:TT-S-100-300	130{J}	81{S}	120{S}	105	89	1.60	1.08	1.24	1.46
G5-25-2H20:TT-S-75-200	117{J}	82{S}	72{S}	60	104	1.43	1.63	1.96	1.13
G5-25-2H20:TT-S-150-200	213{J}	145{S}	174{S}	145	155	1.47	1.22	1.47	1.37
G5-25-2H20:TT-S-200-200	261{J}	139{S}	217{S}	203	163	1.88	1.20	1.29	1.60
G5-24-2H20:TT-150-200	201{J}	97{S}	142{S}	118	130	2.06	1.42	1.71	1.55
Mean						1.81	1.44	1.53	1.26
S.D.						0.353	0.335	0.427	0.135
5% quantile standard normal						1.23	0.89	0.83	1.04
5% quantile log normal						1.29	0.96	0.94	1.05

Table 5: Flexural specimens predicted characteristic strength

Test ID	M_{test} (kNm) {failure mode}	$M_{\text{k,STM1}}$ (kNm)	$M_{\text{k,STM2}}$ (kNm)	$M_{\text{k,UB}}$ (kNm)	$M_{\text{k,FEA}}$ (kNm)	$\frac{M_{\text{test}}}{M_{\text{k,STM1}}}$	$\frac{M_{\text{test}}}{M_{\text{k,STM2}}}$	$\frac{M_{\text{test}}}{M_{\text{k,UB}}}$	$\frac{M_{\text{test}}}{M_{\text{k,FEA}}}$
B2-26-2H20-S-0	111{J}	63	56	45	69	1.76	1.97	2.47	1.61
B2-39-2H20-S-0	129{Y}	89	94	79	98	1.44	1.37	1.64	1.31
B2-24-2H20-/-0	84{J}	30	45	36	55	2.79	1.87	2.32	1.52
B2-26-2H20-S-10	99{J}	56	50	40	70	1.77	2.00	2.48	1.41
Mean						1.94	1.80	2.23	1.46
C.o.V.						0.262	0.141	0.154	0.078

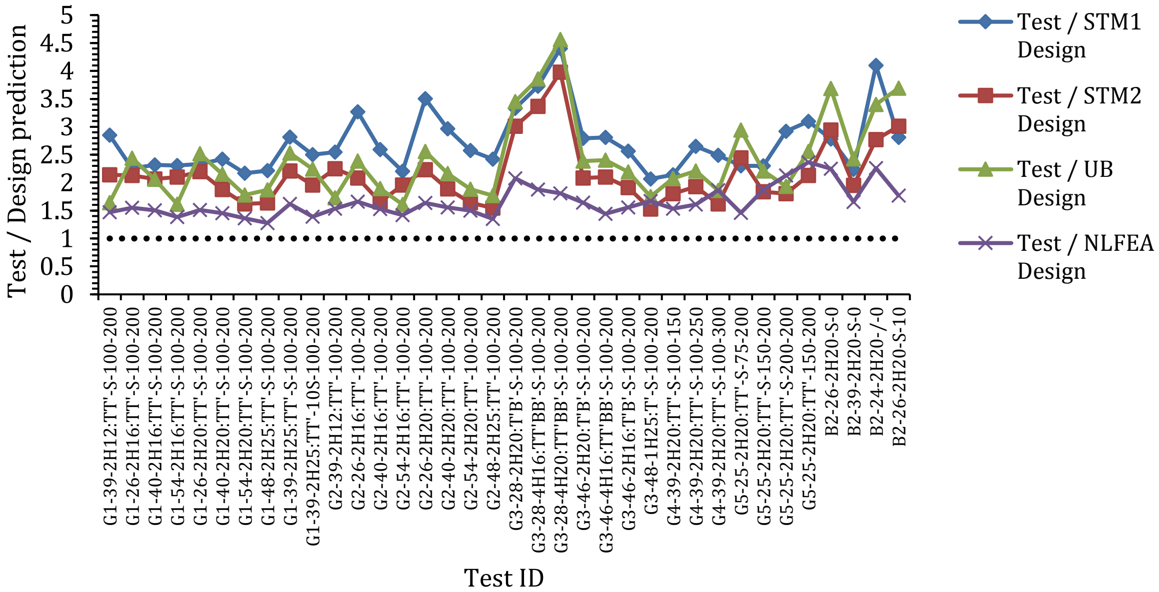

Figure 10: Design joint strength predictions from analytical models and NLFEA

4.2. Design recommendations

Of the analytical design methods, STM2 is recommended due to its simplicity and relative economy. However, for specialist applications design by testing in conjunction with NLFEA parametric studies has the potential for significant economies. Ratios of measured to predicted joint design strengths calculated with EC2 partial factors of γ_c = 1.5 for concrete and γ_s = 1.15 for reinforcement are compared in Figure 10.

The following observations from tests and NLFEA should be taken into consideration in the design of headed bar joints with the tested configuration.

- Placing transverse bars above and below the lapped headed bars increases joint strength and stiffness compared with placing bars on one side only;
- Additional strength and ductility are achieved by using four instead of two transverse bars;
- For a required transverse bar cross-sectional area, providing several smaller diameter bars improves joint performance compared with a single large diameter bar;
- Placing transverse bars closer to the longitudinal bar heads improves the performance of longer laps;
- The provision of transverse shear studs with diameter of at least 10 mm increases the strength of tension laps by up to 30% with the increase greatest for low concrete strengths.

- Shear studs can be omitted in tension specimens with lap length increased in compensation. This may be possible in flexural joints but requires further investigation since shear studs restrain flexural prying action which increases with lap length;
- Joint strength appears relatively insensitive to out-of-plane construction tolerances of up to 10 mm.

Table 6 gives transverse bar sizes and concrete strengths required by each analytical method for headed bars to reach their design yield strength (i.e. with partial factors of γ_c = 1.5 and γ_s = 1.15). Results are provided for headed bars of 16 mm, 20 mm and 25 mm diameter spaced at 200 mm centres with laps of 100 mm and 150 mm. Reinforcement is assumed to have a characteristic strength of 500 MPa.

In all cases, STM1 requires the highest concrete strength for headed bar yield and STM2 the least. The UB model requires least transverse bar area since the STM configuration in Figure 5 requires transverse bars to be provided in the TB positions due to reversal of forces between alternate transverse bars in long joints. The highly complex stress distributions within the joint are not easily captured by analytical models, but are represented relatively well by NLFEA. It is therefore suggested that design or assessment can alternatively be based on NLFEA simulations, provided that a suitable safety format is adopted such as the ECOV method of MC2010. The transverse bar predictions for 20 mm and 16 mm headed bars should be validated by limited testing since only 25 mm headed bars were tested in this study.

Table 6: Required transverse bars and concrete strength for headed bar yield

		100 mm lap		150 mm lap	
	Analytical model	Transverse bars	f_{ck} (MPa)	Transverse bars	f_{ck} (MPa)
H25 headed bars H10 shear studs	STM1	2H16:T'B'	82	2H12:T'B'	49
	STM2	2H16:T'B'	54	2H12:T'B'	31
	Upper bound	2H16	63	2H16	38
H25 headed bars no shear studs	STM1	2H16:T'B'	99	2H12:T'B'	53
	STM2	2H16:T'B'	64	2H12:T'B'	37
	Upper bound	2H16	74	2H16	44
H20 headed bars H10 shear studs	LOR STM	1H20:T'	63	2H10:T'B'	36
	STM12	1H20:T'	41	2H10:T'B'	23
	Upper bound	2H12	57	2H12	30
H20 headed bars no shear studs	STM1	1H20:T'	82	2H10:T'B'	43
	STM2	1H20:T'	48	2H10:T'B'	27
	Upper bound	2H12	67	2H12	37
H16 headed bars H10 shear studs	STM1	1H16:T'	49	1H12:T'	27
	STM2	1H16:T'	35	1H12:T'	18
	Upper bound	2H12	43	2H10	26
H16 headed bars no shear studs	STM1	1H16:T'	69	1H12:T'	36
	STM2	1H16:T'	41	1H12:T'	21
	Upper bound	2H12	50	2H10	30

5. Practical applications of the e6 floor system

5.1. Two Fifty One

The Two Fifty One project is a mixed use development comprising of a two level basement box, 41-storey residential tower and an adjacent eight-storey commercial building. The residential tower has successfully embraced the principles of Design for Manufacture and Assembly (DfMA) such that 72% of the frame and facade is manufactured offsite. The structure extends to 131 m in height and is the first ever to be built using the e6 system. Use of the e6 system has ultimately delivered greater certainty and improved cost, programme, quality, safety and logistics.

In total, the Two Fifty One superstructure (frame and façade) is a kit of 7,282 prefabricated precast concrete elements. The vertical structure is formed using three principal components; precast concrete columns, a twinwall core and solidwall stair and lift shafts. The horizontal structure is then constructed using a combination of solid balcony slabs, lattice slab and Laing O'Rourke's patented e6H system. The e6 joint system at Two Fifty One is used to connect reinforced concrete edge beams (primary span) with pre-stressed hollowcore planks that incorporate full length headed reinforcement bars within intermittent fully grout filled cores, resulting in a headed bar spacing of 242 mm. Headed bars used are 16 mm in diameter with 50x12 mm circular friction-welded heads extending 170 mm from the precast elements, resulting in a 116 mm lap length within a 200 mm wide joint. 16 mm shear studs are also installed in the joint before casting the C60/75 grade concrete insitu infill. A typical joint detail is shown in Figure 11.

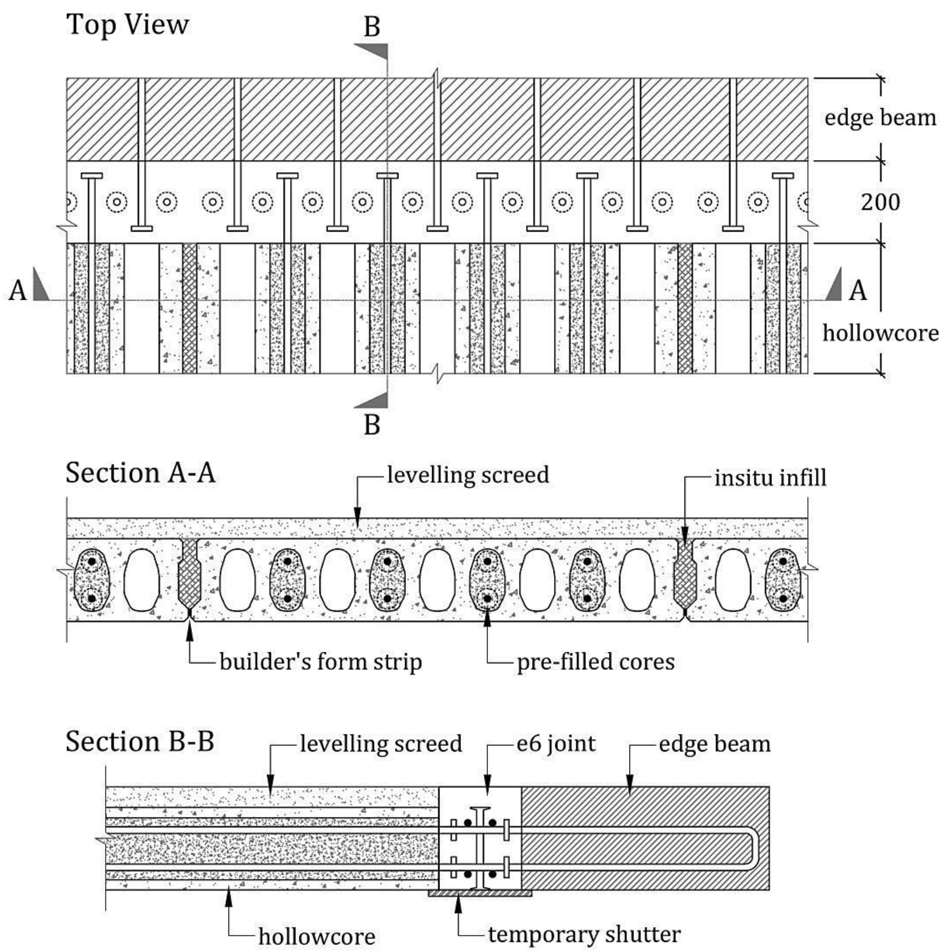

Figure 11: Typical e6 joint details at Two Fifty One

Figure 12: View of Two Fifty One during construction

At Two Fifty One the construction team were able to construct a floor every six days, however, as part of the smarter construction methodology adopted, this 6 day cycle also included for one day of prefabricated bathroom pod lifting, and half a day window frame lifting. The fact that the team were able to load out the slab with pods and frames was a result of having minimal propping and sufficient strength developed in the joints within 24 hours of casting. Figure 12 shows a typical 920 m^2 plate at Two Fifty One with the propping and bathroom pods installed.

Overall the rapid and virtually prop free construction methodology has enabled a smarter prefabricated MEP (mechanical, electrical and plumbing systems) and fit-out solution. The project has modularised and part commissioned key MEP components off-site. Furthermore, of the 515 bathrooms required, 499 have been manufactured in a factory environment and installed with the structure as it progresses, helping reduce the demands on labour and programme while helping maintain the line of balance (continuity of trades) during fit-out.

As part of Laing O'Rourke's drive for smarter, more efficient construction methodologies each new innovation or technology is developed in line with their 70:60:30 agenda. Whereby 70% of frame, facade and MEP are delivered using off-site prefabricated products; resulting in a 60% reduction in the on-site workforce, achieving a 30% reduction in programme. To date, the Two Fifty One project is the closest of any projects to achieving these metrics as demonstrated in Table 7.

Table 7: Frame performance; DfMA vs Traditional on Two Fifty One

Description		Floor Cycle	Total Operative Days	Operatives per Week	Total Days
DfMA Solution	40 Floors	6 day	6720	28	240
Insitu Solution	40 Floors	9 day	13320	37	360
Variance	-	-	6600	9	120
Reduction/Saving	-	-	50%	24%	33%
70% of the Frame and practical MEP systems designed for offsite manufacture					

5.2. Potential impact of research in practice

It is hoped that the greater understanding of joint behaviour achieved through this research will make it possible for LOR to increase client confidence in the e6 system and demonstrate its benefits when compared to other construction systems. Design of e6 joints in practice has so far been done following STM1, backed up by limited testing. As demonstrated in this research, this leads to safe joint designs, which could however be overly conservative. Joint designs can be optimised by taking into consideration findings from this research and making use of proposed alternative design approaches. As an example, a preliminary cost analysis on the Two Fifty One project has shown that, by simply eliminating the installation of shear studs while increasing joint width to 250 mm in compensation, savings of approximately 20% in cost and 50% in man hours associated with the e6 joints could be achieved. These would translate to roughly 2% and 6% savings in total superstructure cost and on-site labour respectively. It has also been shown that lower joint concrete strengths than currently used in practice could be sufficient to achieve well-performing joints, especially if joints are placed away from regions subjected to large bending moments. In view of building life cycle, the lower the required joint concrete strength, the easier it will be in the case that the structure would need to be dismantled by breaking away the joint concrete by means of techniques such as hydro-cutting.

6. Conclusions

This paper describes research carried out at Imperial College London into headed bar splice joints between precast concrete slabs. Tests were done on tension and flexural specimens of a similar configuration used by Laing O'Rourke in their patented e6 floor system. The tests investigated the influence on headed bar lap strength and stiffness of joint geometry, insitu concrete strength, size and arrangement of transverse reinforcement, shear studs and out-of-plane tolerances. Tests showed that a 100 mm lap in 28 MPa cylinder strength concrete with four H16 transverse bars and H10 shear studs was sufficient to achieve yield of 25 mm headed bars. Flexural yield and significant ductility were achieved using 39 MPa cylinder strength joint concrete with two top 20 mm transverse bars and 12 mm shear studs.

Nonlinear finite element models and analytical models based on strut-and-tie and upper bound plasticity were developed for use in the design of headed bar joints of the configuration tested in this study. Applications of the proposed models for other joint arrangements should be validated by some testing.

The benefits of using the e6 system in precast concrete structures include improvements in buildability and quality control, while reducing construction time, material waste and on-site labour resulting in safer construction sites as highlighted in an example of the recently completed Two Fifty One development by LOR. Observations from this study and use of the proposed analytical models could lead to more optimised joint designs, further reducing costs and on-site labour whilst providing opportunities for better building life cycle management.

7. Acknowledgements

This research project was funded by Laing O'Rourke. The authors would like to thank Arup for their collaboration in this project.

8. References

1. Vella, J.P., *Development of Novel Connection Methods between Precast Concrete Panels*, in *Department of Civil and Environmental Engineering*. 2017, Imperial College London: London. p. 344.
2. Brooker, O., *Use of Headed Bars as Anchorage to Reinforcement.* The Structural Engineer, 2013: p. 49-57.
3. fib, *fib Model Code for Concrete Structures 2010*. 2013. p. 402.

4. Thompson, M.K., Ledesma, A., Jirsa, J.O., and Breen, J.E., *Lap Splices Anchored by Headed Bars.* ACI Structural Journal, 2006. **103**(2): p. 271-279.

5. Thompson, M.K., Jirsa, J.O., and Breen, J.E., *Behaviour and Capacity of Headed Reinforcement.* ACI Structural Journal, 2006. **103**(4): p. 522-530.

6. Chun, S.C., *Lap Splice Tests Using High-Strength Headed Bars of 550 MPa (80 ksi) Yield Strength.* ACI Structural Journal, 2015. **112**(6): p. 679 - 688.

7. Li, L., Ma, Z., Griffey, M.E., and Oesterle, R.G., *Improved Longitudinal Joint Details in Decked Bulb Tees for Accelerated Bridge Construction: Concept Development.* Journal of Bridge Engineering, 2010. **15**(3): p. 327-336.

8. Li, L., Ma, Z., and Oesterle, R.G., *Improved Longitudinal Joint Details in Decked Bulb Tees for Accelerated Bridge Construction: Fatigue Evaluation.* Journal of Bridge Engineering, 2010. **15**(5): p. 511-522.

9. Li, L. and Jiang, Z., *Flexural Behavior and Strut-and-tie Model of Joints with headed bar details Connecting Precast Members.* Perspectives in Science, 2016. **7**: p. 253-260.

10. Dragosavic, M., van den Beukel, A., and Gijsbers, F.B.J., *Loop Connections between Precast Concrete Components Loaded in Bending.* Heron, 1975. **20**(3): p. 36.

11. Gordon, S.R. and May, I.M., *Development of In-situ Joints for Pre-cast Bridge Deck Units.* Proceedings of the Institution of Civil Engineers: Bridge Engineering, 2006. **159**(BE1): p. 17-30.

12. Ong, K.C.G., Hao, J.B., and Paramasivam, P., *A Strut-and-Tie Model for Ultimate Loads of Precast Concrete Joints with Loop Connections in Tension.* Construction and Building Materials, 2005. **20**(3): p. 169-176.

13. Ma, Z.J., Lewis, S., Cao, Q., He, Z., Burdette, E.G., and French, C.E.W., *Transverse Joint Details with Tight Bend Diameter U-Bars for Accelerated Bridge Construction.* Journal of Structural Engineering, 2012. **138**(6): p. 697-707.

14. He, Z., Ma, Z.J., Chapman, C.E., and Liu, Z., *Longitudinal Joints with Accelerated Construction Features in Decked Bulb-Tee Girder Bridges: Strut-and-Tie Model and Design Guidelines.* Journal of Bridge Engineering, 2013. **18**(5): p. 372-379.

15. Joergensen, H.B. and Hoang, L.C., *Tests and Limit Analysis of Loop Connections between Precast Concrete Elements Loaded in Tension.* Engineering Structures, 2013. **52**: p. 558-569.

16. Joergensen, H.B. and Hoang, L.C., *Strength of Loop Connections between Precast Bridge Decks Loaded in Combined Tension and Bending.* Structural Engineering International, 2015. **25**(1): p. 71-80.

17. Vella, J.P., Vollum, R.L., and Jackson, A., *Investigation of Headed Bar Joints between Precast Concrete Panels.* Engineering Structures, 2017. **138**: p. 351-366.

18. Vella, J.P., Vollum, R.L., and Jackson, A., *Flexural Behaviour of Headed Bar Connections between Precast Concrete Panels.* Construction and Building Materials, 2017. **154**: p. 236-250.

19. BSI, *Eurocode 2: Design of concrete Structures - Part 1-1: General Rules and Rules for Buildings*. 2004, British Standards Institution. p. 225.

20. ACI, *Building Code Requirements for Structural Concrete (ACI 318-14) and Commentary*. 2014, American Concrete Institute Committee 318. p. 519.

21. Tuchscherer, R., Birrcher, D., Huizinga, M., and Bayrak, O., *Confinement of Deep Beam Nodal Regions.* ACI Structural Journal, 2010. **107**(6): p. 709-717.

22. fib, *Design of Anchorages in Concrete*. 2011, International Federation for Structural Concrete. p. 265.

23. Cervenka, V., Cervenka, J., Janda, Z., and Pryl, D., *ATENA Program Documentation, Part 8: User's Manual for ATENA-GiD Interface*. 2014, Cervenka Consulting: Prague. p. 112.

24. Vella, J.P., Vollum, R.L., and Jackson, A., *Numerical Modelling of Headed Bar Joints subjected to Tension.* Magazine of Concrete Research, 2017. **69**(20): p. 1027-1042.

25. BSI, *Eurocode 0: Basis of Structural Design*. 2002, British Standards Institution. p. 120.

26. Kueres D, Siburg C. Herbrand M, Classen M, Hegger J, *Uniform Design Method for punching shear in flat slabs and column bases*, Engineering Structures, 2017, **136**, p. 149-164